AD-A265 906

WL-TR-93-4060

# ANALYTICAL MODELS FOR DESCRIBING TH MECHANICAL BEHAVIOR OF FIBER REINFORCED

DR. JAMES M. WHITNEY

UNIVERSAL TECHNOLOGY CORP.
4031 COLONEL GLENN HWY
DAYTON OH 45431-1600

SEPTEMBER 1992

FINAL REPORT FOR 06/01/92-09/30/92

APPROVED FOR PUBLIC RELEASE; DISTRIBUTION IS UNLIMITED.

DTIC
ELECTE
JUN 17 1993
S E D

MATERIALS DIRECTORATE
WRIGHT LABORATORY
AIR FORCE MATERIEL COMMAND
WRIGHT PATTERSON AFB OH 45433-7734

93-13638

NOTICE

When Government drawings, specifications, or other data are used for any purpose other than in connection with a definitely Government-related procurement, the United States Government incurs no responsibility or any obligation whatsoever. The fact that the government may have formulated or in any way supplied the said drawings, specifications, or other data, is not to be regarded by implication, or otherwise in any manner construed, as licensing the holder, or any other person or corporation; or as conveying any rights or permission to manufacture, use, or sell any patented invention that may in any way be related thereto.

This report is releasable to the National Technical Information Service (NTIS). At NTIS, it will be available to the general public, including foreign nations.

This technical report has been reviewed and is approved for publication.

Richard B. Hall

RICHARD B. HALL
Materials Research Engineer
Mechanics & Surface Interactions Branch

L. Scott Theibert

L. SCOTT THEIBERT, Chief
Mechanics & Surface Interactions Branch
Nonmetallic Materials Division

Charles E. Browning

CHARLES E. BROWNING, Chief
Nonmetallic Materials Division
Materials Directorate

If your address has changed, if you wish to be removed from our mailing list, or if the addressee is no longer employed by your organization please notify WL/MLBM, WPAFB, OH 45433-7734 to help us maintain a current mailing list.

Copies of this report should not be returned unless return is required by security considerations, contractual obligations, or notice on a specific document.

# REPORT DOCUMENTATION PAGE

Form Approved
OMB No. 0704-0188

Public reporting burden for this collection of information is estimated to average 1 hour per response, including the time for reviewing instructions, searching existing data sources, gathering and maintaining the data needed, and completing and reviewing the collection of information. Send comments regarding this burden estimate or any other aspect of this collection of information, including suggestions for reducing this burden, to Washington Headquarters Services, Directorate for Information Operations and Reports, 1215 Jefferson Davis Highway, Suite 1204, Arlington, VA 22202-4302, and to the Office of Management and Budget, Paperwork Reduction Project (0704-0188), Washington, DC 20503

**1. AGENCY USE ONLY** *(Leave blank)*

**2. REPORT DATE**
April 1993

**3. REPORT TYPE AND DATES COVERED**
Final Jun 92 - Sep 92

**4. TITLE AND SUBTITLE**
Analytical Models for Describing the Mechanical Behavior of Fiber Reinforced Composites

**5. FUNDING NUMBERS**
C: F33615-89-C-5609
PE 62102F
PR 2418
TA 04
WU 68

**6. AUTHOR(S)**
Dr. James M. Whitney

**7. PERFORMING ORGANIZATION NAMES(S) AND ADDRESS(ES)**
Universal Technology Corp., 4031 Colonel Glenn Hwy., Dayton OH 45431-1600
Dr. James M. Whitney, University of Dayton, Dayton OH 45469-0001

**8. PERFORMING ORGANIZATION REPORT NUMBER**

**9. SPONSORING / MONITORING AGENCY NAME(S) AND ADDRESS(ES)**
WL/MLBM
2941 P St Ste 1
Wright-Patterson AFB OH 45433-7750

**10. SPONSORING / MONITORING AGENCY REPORT NUMBER**
WL-TR-93-4060

**11. SUPPLEMENTARY NOTES**
Work performed by J. M. Whitney under subcontract to UTC.

**12a. DISTRIBUTION / AVAILABILITY STATEMENT**
Approved for public release; distribution is unlimited.

**12b. DISTRIBUTION CODE**

**13. ABSTRACT** *(Maximum 200 words)*
This report covers three topics in mechanics of advanced composites: effect of fiber cross-section on stiffness and strength of laminated composites; failure criteria for composites under combined loading; and stress analysis models for thick composites.

In the area of fiber cross-sectional effect, micromechanics analysis addresses the effect of elliptical fibers on the stiffness and in-plane stress concentrations. Numerical results show that fiber cross-sectional geometry has only a modest influence on laminate elastic constants.

The second topic addresses the interaction between longitudinal compression and transverse loading (tension and compression). Data obtained with a mini-sandwich beam are used to generate failure stresses. Classical lamination theory, including thermal residual stresses due to cure, is utilized for determining ply stresses. Experimental results reveal little interaction between longitudinal compression and transverse stresses as long as the transverse load is below uniaxial transverse failure.

Under the topic of thick composites, the effect of shear deformation and transverse normal stress on the cylindrical bending of laminated, anisotropic plates subjected to a uniform lateral load is investigated. Closed form solutions indicate that the effect of transverse normal stress on maximum deflection is small, even for relatively thick plates.

**14. SUBJECT TERMS**
Composites, micomechanics, elliptical fibers, failure criteria, thick composites, combined loading, compression, shear deformation, and mini sandwich beam.

**15. NUMBER OF PAGES**
42

**16. PRICE CODE**

**17. SECURITY CLASSIFICATION OF REPORT**
UNCLASSIFIED

**18. SECURITY CLASSIFICATION OF THIS PAGE**
UNCLASSIFIED

**19. SECURITY CLASSIFICATION OF ABSTRACT**
UNCLASSIFIED

**20. LIMITATION OF ABSTRACT**
UL

# TABLE OF CONTENTS


Introduction ..... 1

1. Effect of Fiber Cross-Section on Stiffness and Strength of Laminated Composites ... 2

Micromechanics Model for Elliptic Fibers ..... 2

Determination of the Shear Moduli $G_{12}$ and $G_{13}$ ..... 8
Determination of the Shear Modulus $G_{23}$ ..... 10
Stress Concentration Factor at the Fiber/Matrix Interface ..... 11
Numerical Results ..... 12

Laminate Analysis ..... 13

Inplane Elastic Constants ..... 14
Elastic Constants Under Bending ..... 14
Numerical Results ..... 15

2. Failure Criteria for Composites Under Combined Load

Experimental ..... 19

Materials ..... 19
Fabrication of Sandwich Panels ..... 20
Compression Testing of Sandwich Panels ..... 20
Data Reduction ..... 20

Results and Discussion ..... 22

3. Stress Analysis Models for Thick Composites ..... 27

Modified Shear Deformation Theory ..... 27

Cylindrical Bending Under Uniform Lateral Load ..... 31

Numerical Results ..... 35
Discussion ..... 36

References ..... 37



DTIC QUALITY INSPECTED 2

Accesion For
NTIS CRA&I ☒
DTIC TAB ☐
Unannounced ☐
Justification
By
Distribution /
Availability Codes
Dist | Avail and / or Special
A-1

# INTRODUCTION

This report covers three topics relative to mechanics issues in advanced composites: effect of fiber cross-section on stiffness and strength of laminated composites; failure criteria for composites under combined loading; and stress analysis models for thick composites. The work was performed for WL/MLBM, Wright-Patterson, OH 45433-6533 under Contract F33615-89-C-5609 with Universal Technology Corporation. Dr. Richard Hall was the project monitor.

In the area of fiber cross-sectional effect, work is concentrated on looking at the effect of elliptical fibers on the stiffness and inplane stress concentrations at the micromechanics level. Calculated ply stiffness properties are used in conjunction with classical laminated plate theory to determine the effect of fiber geometry on laminate inplane and bending stiffness. The micromechanics model is based on a strength-of-materials approach in conjunction with a laminate analogy. All nine elastic constants of the unidirectional composite are determined. Numerical results show that fiber cross-sectional geometry has only a modest influence on laminate elastic constants.

Failure criteria for filament dominated laminates subjected to compression loading is given consideration under the second topic. Of particular interest is the interaction between longitudinal compression loading and transverse loading (tension and compression). Data obtained in conjunction with a mini-sandwich beam are used to generate failure stresses. Classical lamination theory, including thermal residual stresses due to cure, is utilized for determining ply stresses. Residual stresses are based on initial elastic properties, while mechanical stresses are based on secant modulus at failure (compression stress-strain curve for both unidirectional and laminated composites is nonlinear at high strain levels). Experimental results reveal little interaction between longitudinal compression and transverse stresses as long as the transverse load is below uniaxial transverse failure. A technical paper on this work was presented at the American Society for Composites Conference held at Penn State University, October 13-15, 1992. The paper also appeared in the conference proceedings published by Technomic Publishing Co., Lancaster, PA.

Under the topic of thick composites, the effect of shear deformation and transverse normal stress on the cylindrical bending of laminated, anisotropic plates subjected to a uniform lateral load is investigated. Field equations are based on Reissner's principle in a modified form which requires assumed interlaminar shear and normal stress distributions in addition to the inplane displacements. Closed form solutions are presented for laminates with simply-supported boundaries. Numerical results indicate that the effect of transverse normal stress on maximum deflection is small, even for relatively thick plates.

# 1. EFFECT OF FIBER CROSS-SECTION ON STIFFNESS AND STRENGTH OF LAMINATED COMPOSITES

The effect of fibers with elliptical cross-section shape on composite stiffness and local strength is investigated. Analysis is accomplished at both the micromechanics and macromechanics (laminate) level. At the micromechanics level a strength-of-materials model based on a laminate analogy is utilized to determine the nine elastic constants of a unidirectional composite containing continuous fibers with elliptical cross-section shape. The stress concentration factor at the fiber-matrix interface under transverse normal stress and inplane shear stress is also determined. The effect of fiber geometry on these stiffness properties of laminates under inplane and bending loads are then investigated using the results of the micromechanics model in conjunction with classical laminated plate theory. Stiffness results are compared using a $[0°/\pm 45°]_S$ laminate geometry in conjunction with plies containing various combinations of circular and elliptic fibers.

## Micromechanics Model for Elliptic Fibers

Consider a continuous unidirectional composite containing fibers with an elliptical cross-section. A repeating element of the composite cross-section is assumed to be of the form shown in Fig. 1. Because of symmetry it is only necessary to consider an upper

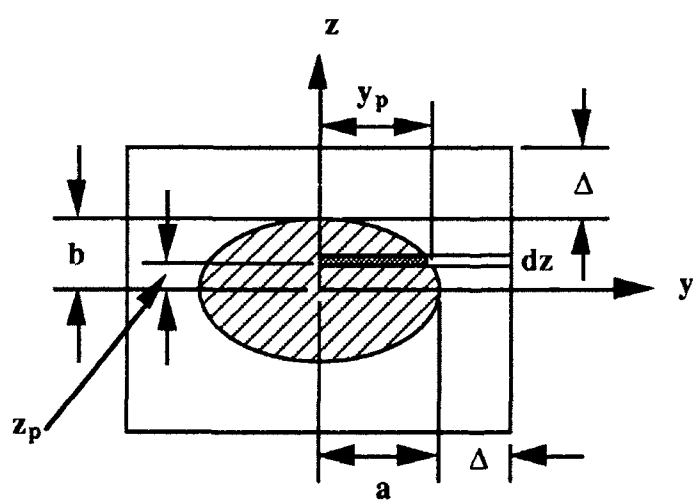


**Figure 1. Analytical micromechanics model.**

quarter of this cross-section in the analysis. This upper quarter is divided into a series of plates (or plies) of thickness dz. Using a strength-of-materials micromechanics approach the stiffnesses of each of these plies are determined as a function of fiber properties, matrix properties, fiber volume fraction, and fiber geometry. The dimension $\Delta$ can be determined as a function of a/b and the volume fraction of fiber, $V_f$, as follows

$$\Delta = \frac{b}{2}\left[-(R+1) + \sqrt{(R+1)^2 + \left(\frac{\pi}{V_f} - 4\right)}\right] \tag{1}$$

where R = a/b.

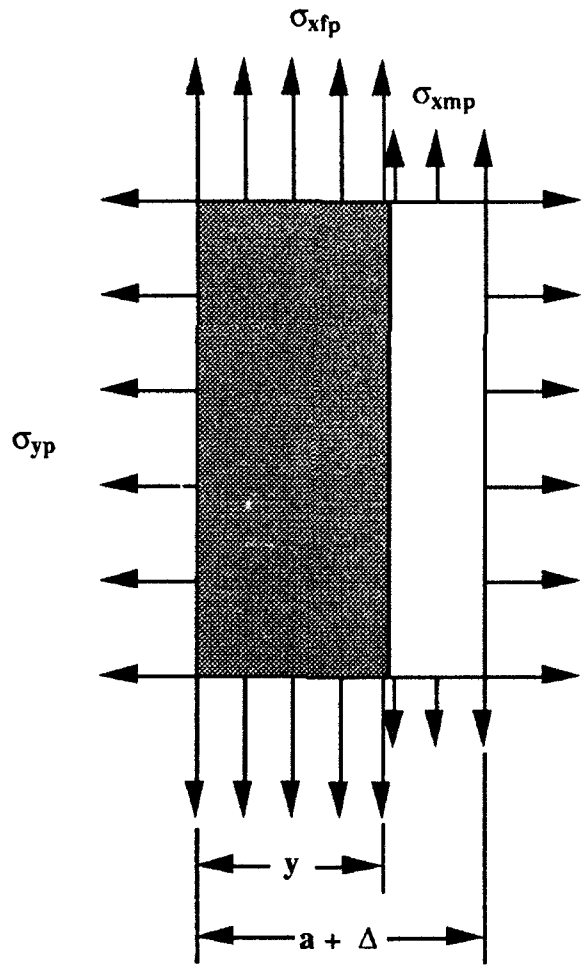


**Figure 2. Ply with biaxial normal stress loading**

A laminate is then constructed from these plies and the resulting stiffnesses determined by integrating the ply properties. The effective elastic constants are determined in the same manner as for a laminated plate [1]. This procedure is referred to as the *laminate analogy micromechanics model* for determining elastic constants of a unidirectional composite. This is an extension of a model proposed by Eckvall [2] for transverse modulus and inplane shear modulus of a unidirectional composite containing circular fibers in a square array [2]. A similar model was used by Chamis [3] for determining the fiber-matrix interface stress concentration factor under transverse tensile (or compression) load and inplane shear load.

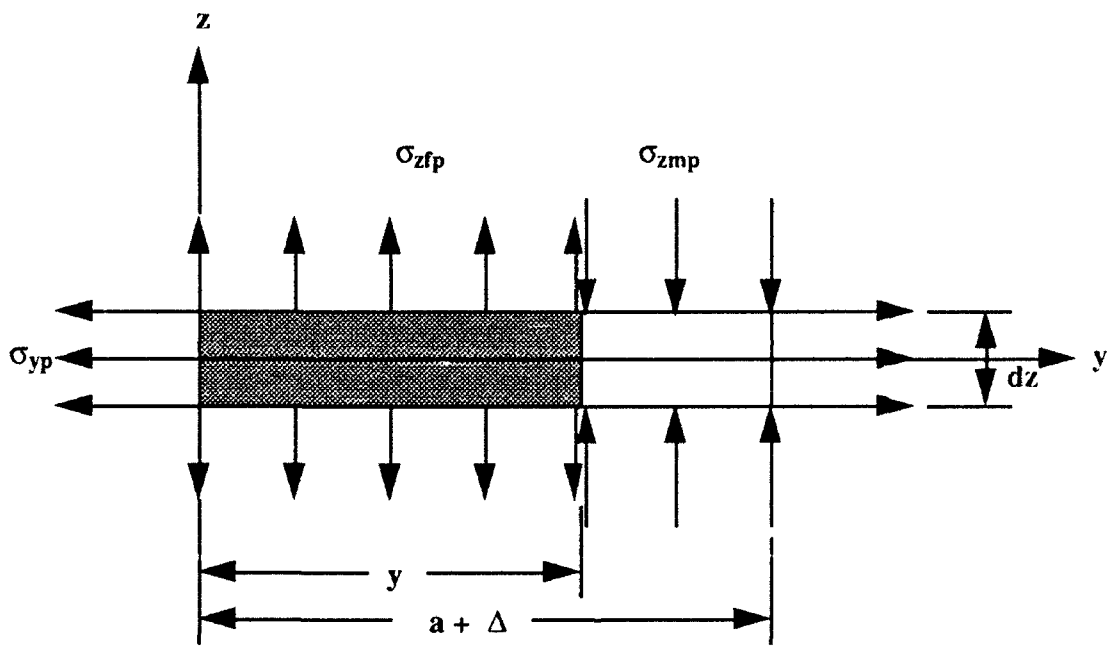


**Figure 3. Through-the-thickness ply loading.**

We now consider the strip shown in Fig. 2 for the ply analysis. The subscripts f, m, and p refer to fiber, matrix, and ply, respectively. Elastic moduli and Poisson's ratios are determined by assuming the volume average inplane ply strains $\varepsilon_x$ and $\varepsilon_y$ to be constant through-the-thickness, i.e we assume

$$\varepsilon_{xp} = \varepsilon_x^0 = \text{constant}, \quad \varepsilon_{yp} = \varepsilon_y^0 = \text{constant} \tag{2}$$

Axial and transverse stresses are assumed to be applied and will vary from ply-to-ply because of the change in local ply stiffness. Because of continuity requirements at the fiber-matrix interface

$$\sigma_{yfp} = \sigma_{ymp} = \sigma_{yp} \tag{3}$$

Through-the-thickness ply loading is shown in Fig. 3. The total load produced by $\sigma_{zp}$ is assumed to vanish, i.e. there is no normal force transmitted through-the-thickness. Thus,

$$\sigma_{zfp}V_{fp} + \sigma_{zmp}(1-V_{fp}) = 0 \tag{4}$$

where $V_{fp}$ is the volume fraction of fiber in the ply, i.e.

$$V_{fp} = \frac{y_p}{(a + \Delta)} \tag{5}$$

and

$$y_p = a\sqrt{1 - \left(\frac{z_p}{b}\right)^2}$$

Assuming a transversely isotropic fiber and an isotropic matrix the stress-strain relations for the constituents are of the form

$$\begin{aligned}
\sigma_{xfp} &= C_{11f}\varepsilon_x^0 + C_{12f}(\varepsilon_{yfp} + \varepsilon_{zp}) \\
\sigma_{yp} &= C_{12f}\varepsilon_x^0 + C_{22f}\varepsilon_{yfp} + C_{23f}\varepsilon_{zp} \\
\sigma_{zfp} &= C_{13f}\varepsilon_x^0 + C_{23f}\varepsilon_{yfp} + C_{22f}\varepsilon_{zp} \\
\sigma_{xmp} &= C_{11m}\varepsilon_x^0 + C_{12m}(\varepsilon_{ymp} + \varepsilon_{zp}) \\
\sigma_{yp} &= C_{12m}(\varepsilon_x^0 + \varepsilon_{zp}) + C_{11m}\varepsilon_{ymp} \\
\sigma_{zmp} &= C_{12m}(\varepsilon_x^0 + \varepsilon_{ymp}) + C_{11m}\varepsilon_{zp}
\end{aligned} \tag{6}$$

where $C_{ij}$ are stiffnesses. It should be noted that, although the volume average transverse strain $\varepsilon_{yp}$ is identical from ply to ply, $\varepsilon_{yp}$ is not the strain of the fiber or the matrix. In fact

$$\varepsilon_{yp} = \varepsilon_y^0 = \varepsilon_{yfp}V_{fp} + \varepsilon_{ymp}(1 - V_{fp}) \tag{7}$$

In addition

$$\sigma_{xp} = \sigma_{xfp} V_{fp} + \sigma_{xmp}(1 - V_{fp}) \tag{8}$$

Combining eqs. (4), (7), and (8), with the constitutive relations, eqs. (6), we obtain the following relationships

$$C_{22p} = \frac{C_{22f} C_{11m}}{[C_{11f}(1 - V_{fp})]}$$

$$\frac{C_{12p}}{C_{22p}} = [\frac{C_{12f}}{C_{22f}} V_{fp} + \frac{C_{12m}}{C_{11m}} (1 - V_{fp})], \quad \frac{C_{23p}}{C_{22p}} = [\frac{C_{23f}}{C_{22f}} V_{fp} + \frac{C_{12m}}{C_{11m}} (1 - V_{fp})]$$

$$\hat{Q}_{11p} = Q_{11f} V_{fp} + Q_{11m}(1 - V_{fp}), \quad \hat{Q}_{22p} = Q_{22f} V_{fp} + Q_{11m}(1 - V_{fp})$$

$$\hat{Q}_{12p} = Q_{12f} V_{fp} + Q_{12m}(1 - V_{fp}) \tag{9}$$

$$C_{11p} = [\hat{Q}_{11p} + C_{22p} (\frac{C_{12p}}{C_{22P}})^2], \quad C_{33p} = [\hat{Q}_{22p} + C_{22p} (\frac{C_{23p}}{C_{22P}})^2]$$

$$C_{13p} = [\hat{Q}_{12p} + C_{22p} (\frac{C_{12p}}{C_{22P}})(\frac{C_{23p}}{C_{22P}})]$$

where $Q_{ij}$ are reduced stiffnesses for plane stress. The reduced stiffnesses for the ply can now be determined utilizing the results from eqs. (9). In particular,

$$Q_{11p} = [C_{11p} - \frac{C_{13p}^2}{C_{33p}}], \quad Q_{22p} = [C_{22p} - (\frac{1}{C_{33p}})(C_{22p}^2)(\frac{C_{23p}}{C_{22P}})^2]$$

$$Q_{12p} = [C_{12p} - (\frac{1}{C_{33p}})(C_{22p}^2)(\frac{C_{12p}}{C_{22P}})(\frac{C_{23p}}{C_{22P}})] \tag{10}$$

These reduced stiffnesses are now averaged through-the-thickness to produce effective values for the micromechanics model, i.e.

$$\overline{Q}_{ij} = \frac{1}{(1 + \frac{\Delta}{b})} \int_0^{(1+\frac{\Delta}{b})} Q_{ijp} \frac{dz}{b} \quad (i, j = 1, 2) \tag{11}$$

This integration is performed numerical using 100 strips through-the-thickness. Elastic constants can now be determined in the same manner as in laminated plate theory, i.e.

$$E_1 = \overline{Q}_{11} - \frac{\overline{Q}_{12}^{\,2}}{\overline{Q}_{22}},\ E_2 = \overline{Q}_{22} - \frac{\overline{Q}_{12}^{\,2}}{\overline{Q}_{11}},\ \ \nu_{12} = \frac{\overline{Q}_{12}}{\overline{Q}_{22}} \tag{12}$$

where $E_1$, $E_2$, and $\nu_{12}$ denote the modulus parallel to the fibers, the modulus transverse to the fibers, and the Poisson's ratio as determined from a uniaxial tensile test parallel to the fibers while measuring the strain transverse to the fibers, respectively.

Recognizing that $\sigma_{zp}$ of the ply vanishes and utilizing the ply constitutive relations, we can write

$$\varepsilon_{zp} = -\frac{C_{13p}}{C_{33p}}\,\varepsilon_x^0 - \frac{C_{23p}}{C_{33p}}\,\varepsilon_y^0 \tag{13}$$

Integration of eq. (13) leads to an effective value of the through-the-thickness strain, which can be written in the form

$$\overline{\varepsilon}_z = -\,H_{13}\varepsilon_x^0 - H_{23}\,\varepsilon_y^0 \tag{14}$$

where

$$H_{i3} = \frac{1}{(1+\frac{\Delta}{b})}\int_0^{(1+\frac{\Delta}{b})} \frac{C_{i3p}}{C_{33p}}\frac{dz}{b} \qquad (i = 1, 2)$$

We now consider a uniaxial load applied parallel to the fibers. In this case we have

$$\varepsilon_y^0 = -\,\nu_{12}\,\varepsilon_x^0,\ \ \overline{\varepsilon}_z^0 = -\,\nu_{13}\,\varepsilon_x^0 \tag{15}$$

where, obviously, $\nu_{13}$ denotes the Poisson's ratio as determined from measuring the strain transverse to the fibers during this uniaxial tensile test in the fiber direction. Combining eqs. (14) and (15), and taking into account eq. (12), we find that

$$\nu_{13} = H_{13} - H_{23}\frac{\overline{Q}_{12}}{\overline{Q}_{22}} \tag{16}$$

In a similar manner, measuring the strain through-the-thickness during a uniaxial tensile test transverse to the fibers leads to the Poisson's ratio $\nu_{23}$. In this case we have

$$\varepsilon_x^0 = -\nu_{12}\frac{E_2}{E_1}\varepsilon_y^0, \quad \bar{\varepsilon}_z^0 = -\nu_{23}\,\varepsilon_y^0 \tag{17}$$

Combining eqs. (14) and (17), and taking into account eq. (12), we obtain the result

$$\nu_{23} = H_{23} - H_{13}\frac{\bar{Q}_{12}}{\bar{Q}_{11}} \tag{18}$$

The through-the-thickness modulus, $E_3$, can be calculated by rotating the model in Fig. 1 by 90°, i.e. substituting 1/R for R in the current analysis and letting $E_3 = E_2$.

## Determination of the Shear Moduli $G_{12}$ and $G_{13}$

For determination of the inplane shear modulus $G_{12}$ we consider the ply loading shown in Fig. 4. The effective shear strain, $\gamma_{xyp}$ is assumed to be the same within each ply, i.e.

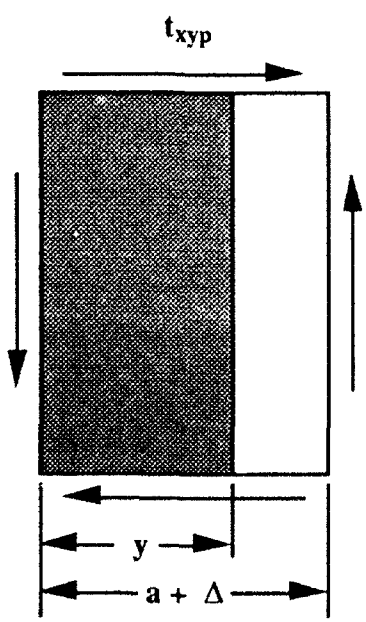


**Fig 4. Inplane shear loading at ply level.**

$$\gamma_{xyp} = \gamma^0_{xy} = \text{constant} \tag{19}$$

where $\gamma^0_{xy}$ is the macroscopic shear strain relative to the x-y plane.

Continuity of the shear stress at the fiber matrix interface requires th

$$\tau_{xyf} = \tau_{xym} = \tau_{xyp} \tag{20}$$

and macroscopic stress-strain relation is of the form

$$\gamma^0_{xy} = \frac{\bar{\tau}_{xy}}{G_{12}} \tag{21}$$

where

$$\bar{\tau}_{xy} = \frac{1}{(1 + \frac{\Delta}{b})} \int_0^{(1+\frac{\Delta}{b})} \tau_{xyp} \frac{dz}{b}$$

The shear strain at the ply level can be shown to be the following function of the fiber and matrix shear strains

$$\gamma_{xyp} = \gamma^0_{xy} = \gamma_{xyf} V_{fp} + \gamma_{xym}(1 - V_{fp}) \tag{22}$$

The constitutive relations for the fiber and matrix are of the form

$$\gamma_{xyf} = \frac{\tau_{xyp}}{G_{12f}}, \quad \gamma_{xym} = \frac{\tau_{xyp}}{G_m} \tag{23}$$

Combining eqs. (22) and (23), we obtain the ply shear modulus

$$G_{12p} = \frac{\tau_{xyp}}{\gamma^0_{xy}} = \frac{G_{12f} G_m}{[G_{12f}(1 - V_{fp}) + G_m V_{fp}]} \tag{24}$$

The shear modulus $G_{12}$ can be obtained by combining eqs. (21) and (24) with the result

$$G_{12} = \frac{1}{(1 + \frac{\Delta}{b})} \int_0^{(1+\frac{\Delta}{b})} \frac{G_{12f}G_m}{[G_{12f}(1 - V_{fp}) + G_m V_{fp}]} \frac{dz}{b} \tag{25}$$

The shear modulus $G_{13}$ can be obtained in the same manner as $E_3$, i.e. Fig. 1 is rotated 90° and the same procedure implemented as for $G_{12}$.

## Determination of the Shear Modulus $G_{23}$

For the transverse shear modulus, $G_{23}$, we consider the through-the-thickness ply loading as shown in Fig. 5. The shear strain at the ply level is assumed to be constant, i.e.

$$\gamma_{yzp} = \gamma_{yzf} = \gamma_{yzm} \tag{26}$$

and the effective ply shear stress is assumed to be constant through-out the thickness of the plate. Thus

$$\tau_{yzp} = \tau_{yz} \tag{27}$$

A simple force balance leads to the result

$$\tau_{yzp} = \tau_{yz} = \tau_{yzf} V_{fp} + \tau_{yzm} (1 - V_{fp}) \tag{28}$$

This relationship does not maintain continuity of $\tau_{yz}$ at the fiber/matrix interface at the ply

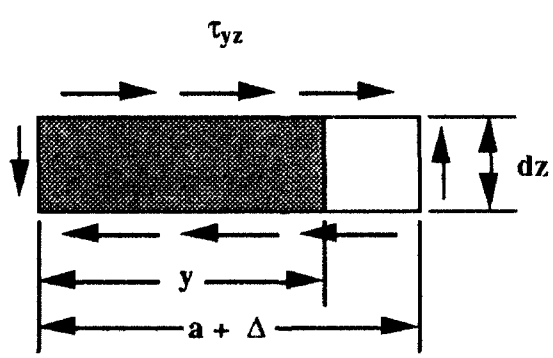


**Figure 5. Through-the-thickness shear loading at ply level**

level. However, if we consider a very steep stress gradient near the fiber/matrix interface, then we can accept eq. (28) on an average stress basis. The constitutive relations are of the form

$$\tau_{yz} = G_{23p}\gamma_{yzp}, \quad \tau_{yzf} = G_{23f}\gamma_{yzp}, \quad \tau_{yzm} = G_m\gamma_{yzp} \tag{29}$$

Substituting eq. (29) into eq. (28), we obtain a simple rule-of-mixtures relationship.

$$G_{23p} = G_{23f}V_{fp} + G_m\,(1 - V_{fp}) \tag{30}$$

The effective laminate shear strain is obtained by integrating $\gamma_{yzp}$ through-the-thickness with the result

$$\bar{\gamma}_{yz} = \frac{\tau_{yz}}{G_{23}} = \frac{\tau_{yz}}{(1 + \frac{\Delta}{b})} \int_0^{(1+\frac{\Delta}{b})} \frac{1}{G_{23p}} \frac{dz}{b} \tag{31}$$

which immediately leads to the relationship

$$G_{23} = \frac{(1 + \frac{\Delta}{b})}{\displaystyle\int_0^{(1+\frac{\Delta}{b})} \frac{1}{[G_{23f}V_{fp} + G_m\,(1 - V_{fp})]} \frac{dz}{b}} \tag{32}$$

We have now determined all 9 elastic constants for the repeating elliptic fiber element.

## Stress concentration Factor at the Fiber/Matrix Interface

The stress concentration factor (SCF) at the fiber/matrix interface is of interest for both transverse and inplane shear loading. For these loadings the maximum stress will occur at $z = 0$, $y = b$. In the scheme under consideration this represents the first element in the integration procedure. Thus, for transverse loading

$$\sigma_{yp}(1) = Q_{12p}(1)\varepsilon_x^0 + Q_{22p}(1)\varepsilon_y^0 \tag{33}$$

where (1) denotes the first element in the integration scheme. Under transverse loading we have

$$\bar{\sigma}_y = E_2 \varepsilon_y^0 \tag{34}$$

Utilizing eqs. (33) and (34) in conjunction with the definition of SCF, and taking into account eq. (17), we obtain the following result

$$SCF = \frac{\sigma_{yp}(1)}{\bar{\sigma}_y} = \frac{[Q_{22p}(1) - \nu_{12}\frac{E_2}{E_1} Q_{12p}(1)]}{E_2} \tag{35}$$

A similar procedure in conjunction with inplane shear loading leads to the following SCF relationship

$$SCF = \frac{\tau_{xyp}(1)}{\bar{\tau}_{xy}} = \frac{G_{12p}(1)}{G_{12}} \tag{36}$$

## Numerical Results

In the results presented here the fiber is assumed to be transversely isotropic and the matrix is assumed to be isotropic. We now consider the following constituent properties

$$\begin{gathered} E_{1f} = 35\text{x}10^6 \text{ psi}, E_{2f} = 3\text{x}10^6 \text{ psi}, G_{12f} = 5\text{x}10^6 \text{ psi}, \nu_{12f} = 0.25 \\ \nu_{23f} = 0.55, E_{1f} = 35\text{x}10^6 \text{ psi}, E_m = 5\text{x}10^5 \text{ psi}, \nu_m = 0.35 \end{gathered} \tag{37}$$

Numerical results are shown in Table 1 for circular fibers and for elliptic fibers with various a/b ratios. The fiber volume fraction is assumed to be 0.6. The fiber properties given by eq. (37) are typical of state-of-the-art graphite fibers and the matrix properties are those of high performance epoxy resins.

The results seem in Table appear to be reasonable. There is, however, an inconsistency relative to $G_{23}$. In particular the same value should be obtained for R and 1/R aspect ratios (e.g. R = 2 and 0.5 should yield the same values). This is not the case with regard to the results shown in Table 1. These values may, however, be considered as upper and lower bounds.

As one would anticipate, elliptical fibers with R > 1 increase the transverse modulus and inplane shear modulus, while the same moduli are reduced for R < 1. The

percentage of these changes are not great. It should be noted, however, that the low transverse modulus and low inplane shear modulus of the fiber contributes to the smaller increase. In particular, the ratio of fiber to matrix property in this case is not significantly large. For a high modulus isotropic fiber, such as boron, the effect of fiber cross-section shape may be more significant.

**TABLE 1 Micromechanics Results ($V_f = 0.6$)**

| | R=1 | R=2 | R=4 | R=1/2 | R=1/4 |
|---|---|---|---|---|---|
| $E_1$ (msi) | 21.190 | 21.190 | 21.190 | 21.190 | 21.190 |
| $E_2$ (msi) | 1.452 | 1.507 | 1.562 | 1.406 | 1.375 |
| $E_3$ (msi) | 1.452 | 1.406 | 1.375 | 1.507 | 1.562 |
| $\nu_{12}$ | 0.289 | 0.286 | 0.282 | 0.293 | 0.296 |
| $\nu_{13}$ | 0.289 | 0.293 | 0.296 | 0.286 | 0.282 |
| $\nu_{23}$ | 0.398 | 0.413 | 0.428 | 0.383 | 0.372 |
| $G_{12}$ (msi) | 0.637 | 0.728 | 0.850 | 0.577 | 0.540 |
| $G_{13}$ (msi) | 0.637 | 0.577 | 0.540 | 0.728 | 0.850 |
| $G_{23}$ (msi) | 0.506 | 0.480 | 0.461 | 0.535 | 0.562 |
| SCF ($\sigma_2$) | 1.456 | 1.540 | 1.621 | 1.384 | 1.332 |
| SCF ($\tau_{12}$) | 1.836 | 2.085 | 2.400 | 1.663 | 1.553 |

It should also be noted that the stress concentration factors at the fiber matrix interface are increased for $R > 1$ and decreased for $R < 1$. Thus, it is anticipated that the transverse strength and inplane shear strength would be effected in a corresponding fashion.

## Laminate Analysis

We now consider the effect of fiber cross-sectional shape on the inplane and bending stiffnesses of laminates. This is accomplished by combining the ply elastic properties produced for various fiber cross-sectional shapes (as given by Table 1) with classical laminated plate theory.

## Inplane Elastic Constants

Inplane elastic constants for symmetric laminates can be determined from classical laminated plate theory by considering the laminate inplane constitutive relations in the form

$$\hat{\sigma}_i = \hat{Q}_{ij}\varepsilon_j^0 \qquad (i, j = 1, 2, 6) \tag{38}$$

where

$$\hat{\sigma}_i = \int_{-h/2}^{h/2} \sigma_i^{(k)}\, dz, \;\; \hat{Q}_{ij} = \int_{-h/2}^{h/2} Q_{ij}^{(k)}\, dz$$

and the superscript k denotes the kth layer. Then the inplane effective laminate elastic constants for balanced laminates (same number of angle-ply layers at $\pm\,\theta$) take the form

$$\begin{gathered} E_x = \hat{Q}_{11} - \frac{\hat{Q}_{12}^{\,2}}{\hat{Q}_{22}}, \;\; E_y = \hat{Q}_{22} - \frac{\hat{Q}_{12}^{\,2}}{\hat{Q}_{11}} \\ G_{xy} = \hat{Q}_{66}, \;\; \nu_{xy} = \frac{\hat{Q}_{12}}{\hat{Q}_{22}} \end{gathered} \tag{39}$$

Balanced laminates produce orthotropic inplane elastic constants (no shear coupling). This is due to the fact that the effective laminate stiffnesses are independent of stacking sequence.

## Elastic Constants Under Bending

Under bending loads, the constitutive relations for a symmetric laminate are of the form

$$M_i = D_{ij}\kappa_j \qquad (i, j = 1, 2, 6) \tag{40}$$

where

$$M_i = \int_{-h/2}^{h/2} \sigma_i^{(k)} z\, dz, \;\; D_{ij} = \int_{-h/2}^{h/2} Q_{ij}^{(k)} z^2\, dz$$

and $\kappa_j$ are plate curvatures. In order to obtain effective elastic constants, we rewrite eq.

(40) in the form

$$M_i = \frac{h^3}{12}\hat{Q}^b_{ij}\kappa_j \tag{41}$$

where the superscript b denotes bending properties. The effective bending stiffnesses are obviously given by

$$\hat{Q}^b_{ij} = \frac{12}{h^3} D_{ij}$$

Inverting eq. (41), we can write the constitutive relations in terms of compliances.

$$\kappa_i = \frac{12}{h^3}\hat{S}^b_{ij}M_j \tag{42}$$

where $S^{(b)}_{ij}$ denote effective bending coampliances of the laminate.

Since the bending stiffnesses, $D_{ij}$, are a function of stacking sequence, the effective stiffnesses for balanced laminates will not be orthotropic. Thus, shear coupling (in the form of bending-twisting coupling) will be present for the general case of symmetric laminates subjected to bending loads. Effective bending elastic constants can be determined from the compliances in eq. (42) in the usual manner, i.e.

$$\begin{aligned} E^b_x &= \frac{1}{S^b_{11}}, \quad E^b_y = \frac{1}{S^b_{22}}, \quad \nu_{xy} = -\, S^b_{12}E^b_x \\ G^b_{xy} &= \frac{1}{S^b_{66}}, \quad \eta^b_x = S^b_{16}E^b_x, \quad \eta^b_y = S^b_{26}E^b_y \end{aligned} \tag{43}$$

where $\eta^b_x$ and $\eta^b_y$ are bending shear coupling coefficients.

## Numerical Results

Elastic constants under inplane and bending loads are shown in Table 2 for a $[0°_2/\pm45°]_S$ laminates. Ply properties are taken from Table 1. Four different combinations of fiber geometries are considered as follows:

#1 All plies with R = 1

#2 0° plies R = 2, 45° plies R = 1

#3 0° plies R = 1/2, 45° plies R = 1

#4 All plies R = 2

#5 All plies R = 1/2

**TABLE 2 Laminate Elastic Constants, $[0°_2/\pm45°]_S$**

| | #1 | #2 | #3 | #4 | #5 |
|---|---|---|---|---|---|
| $E_x$ (Msi) | 11.900 | 11.910 | 11.890 | 12.040 | 11.800 |
| $E_y$ (Msi) | 3.419 | 3.445 | 3.398 | 3.517 | 3.349 |
| $\nu_{xy}$ | 0.711 | 0.708 | 0.714 | 0.689 | 0.727 |
| $G_{xy}$ (Msi) | 3.059 | 3.104 | 3.029 | 3.109 | 3.025 |
| $E_x^b$ (Msi) | 18.910 | 18.910 | 18.900 | 18.940 | 18.890 |
| $E_y^b$ (Msi) | 1.883 | 1.940 | 1.836 | 1.956 | 1.825 |
| $\nu_{xy}^b$ | 0.444 | 0.441 | 0.448 | 0.434 | 0.453 |
| $G_{xy}^b$ (Msi) | 1.136 | 1.218 | 1.081 | 1.220 | 1.079 |
| $\eta_x^b$ | -0.208 | -0.197 | -0.216 | -0.199 | -0.215 |
| $\eta_y^b$ | -0.358 | -0.336 | -0.374 | -0.335 | -0.375 |

As easily seen from Table 2, fiber geometry has little effect on either inplane or bending elastic constants.

## 2. FAILURE CRITERIA FOR COMPOSITES UNDER COMBINED LOADING

The uniaxial compression strength of a 0° composite has long been a property of significant interest to both materials engineers and designers. In the present paper, however, the interaction between longitudinal compression and transverse loading of a 0° composite is investigated. This is accomplished by subjecting a series of laminates with different stacking geometries to inplane compression loading.

Laminate geometries were chosen to produce a number of longitudinal compression to transverse stress ratios. In particular, for multidirectional laminates the 0° plies will be under biaxial loading which creates an interesting challenge relative to failure criteria. For example, consider the three loading conditions shown in Fig. 6. One would anticipate a higher compression strength in the presence of transverse compression loading (Fig. 6b) compared to pure compression (Fig. 6a). However, if the transverse load is tension (Fig. 6c), one would anticipate a lower longitudinal compression strength. We envision that transverse compression would provide additional stability to the longitudinal compression loading, while transverse tension would have the opposite effect. In addition transverse tension could possibly induce longitudinal splitting followed by fiber microbuckling. If the dominate failure mode, however, is fiber failure, then little interaction between longitudinal and transverse load may be anticipated provided the transverse loads are below the uniaxial transverse strength.

The anticipated difference in longitudinal compression strength between the loadings shown in Fig. 6 are not predictable with a number of conventional failure criteria. Maximum stress and maximum strain do not recognize coupling between longitudinal and transverse normal stresses. For criteria which recognize coupling between stress components, such as the quadratic interaction criterion introduced by Tsai and Wu [1], there are also problems which we will now consider. This criterion is of the form

$$\frac{\sigma_L^2}{S_{LT}\,S_{LC}} + \frac{\sigma_T^2}{S_{TT}\,S_{TC}} - \frac{\sigma_L\,\sigma_T}{2\sqrt{S_{LT}\,S_{LC}\,S_{TT}\,S_{TC}}} + \frac{\tau_{LT}^2}{T_{LT}^2} + \left(\frac{1}{S_{LT}} - \frac{1}{S_{LC}}\right)\sigma_L + \left(\frac{1}{S_{TT}} - \frac{1}{S_{TC}}\right)\sigma_T = 1 \tag{44}$$

where $\sigma_L$, $\sigma_T$, and $\tau_{LT}$, are the normal stresses parallel to the fibers, transverse to the

fibers, and inplane shear stress, respectively. The strength parameters $S_{LT}$, $S_{LC}$, $S_{TT}$, $S_{TC}$, and $T_{LT}$, denote tensile strength and compression strength parallel to the fibers, tensile and compression strength transverse to the fibers, and the inplane shear strength, respectively.

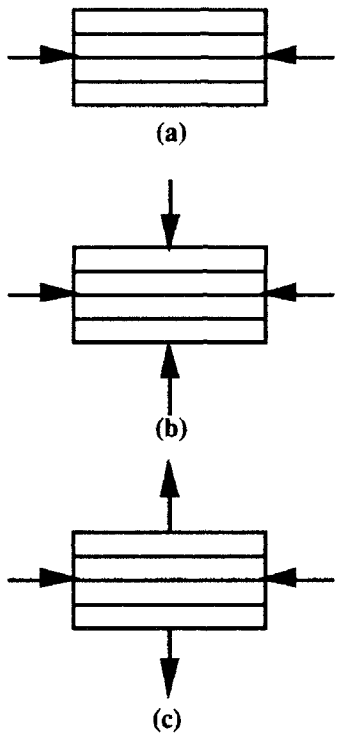


**Fig. 6 Biaxial Loading**

The linear terms and the interaction term between $\sigma_L$ and $\sigma_T$ govern the loading conditions shown in Fig. 6b and 6c. In particular, different results between the loadings in Fig. 6b and 1c depend on a distinct difference between transverse tension and compression strengths and/or differences between longitudinal tension and compression strengths. A recent paper by Theocaris [2] discusses this behavior in some detail. The validity of eq.

(44) in conjunction with the combined loading shown in Fig. 6 will be considered.

## Experimental

Experimental data has been previously obtained by the University of Dayton Research Institute under contract F33 615-92-C-5618 with the Materials Directorate of the Air Force Wright Laboratory. A mini-sandwich specimen [3] consisting of composite face sheets bonded to a neat resin core, as illustrated in Fig. 7, was utilized in obtaining this data. As opposed to the original sandwich beam, which incorporated a honeycomb core, the mini-sandwich specimen is small, relatively inexpensive to fabricate, and uses a smaller volume of material.

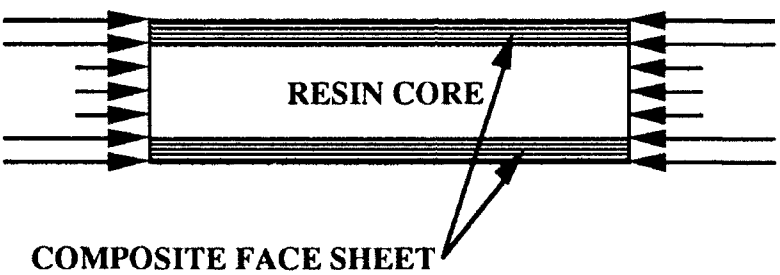


**Fig.7 Mini-Sandwich Beam Specimen**

The mini-sandwich specimen is loaded in a conventional IITRI test fixture (ASTM D-3410) and the data reduced using classical laminated plate theory. The materials, fabrication procedures, and test procedures utilized by the University of Dayton Research Institute are described in the following paragraphs.

### Materials

The cores of the miniature sandwich specimens were fabricated from a neat epoxy resin (Epon 828 from Shell Chemical Co.), cured with Jeffamine D-230 (a polyetheramine from Texaco Inc.). The composite skins were fabricated from a graphite/epoxy AS4/3501-6 prepreg (Hercules, Inc.).

## Fabrication of Sandwich Panels

The miniature sandwich panels were fabricated in a two-step process. In the first step, the following symmetric laminate panels, each 12 in. x 12 in., were first fabricated : $[0]_2$, $[0_2/\pm30]_S$, $[\pm45/0/90]_S$, $[0/45/90/-45]_S$, and $[0/\pm60]_S$. Two plates, each 10 in. x 6 in. were cut from each panel. These were lightly sanded to remove any residual release agent. A mold was constructed by clamping these plates across a uniform Teflon spacer (3.18 mm thick) along three sides to produce a rectangular cavity open at one end. Approximately 125 g of Epon 828 were mixed with 32 phr Jeffamine D-230, and debulked under vacuum to remove entrapped air. The liquid resin was then cast in this mold and allowed to cure at room temperature for 7 days. The product was a symmetric miniature sandwich panel with excellent bonding between composite skin and resin core. In order to measure transverse compression strength, a $[90°]_{24}$ solid panel (no core) was also fabricated.

## Compression Testing of Sandwich Panels

After assuring laminate quality by ultrasonic C-scans, compression tests were performed on specimens cut from these sandwich panels. Specimen sizes were in accordance with ASTM standards for conventional laminates, and tests were also conducted under similar conditions. Axial compression testing was performed in an IITRI fixture on specimens 127 mm long, and 6.4 mm wide. Specimens were gripped through bonded tapered glass/epoxy tabs with a gage length of 12.7 mm. Strain gages were bonded to both faces of each specimen to monitor any bending or buckling resulting from eccentric loading. An additional strain gage was bonded to the side of selected specimens to simultaneously measure axial strain in the core. Tensile tests were also performed on specimens from these panels. Failed specimens were examined in an optical microscope and also in a JEOL JSM 840 scanning electron microscope.

## Data Reduction

Data was reduced using classical laminated plate theory. This procedure involved initial use of macroscopic constitutive relations, which are of the form

$$\begin{bmatrix} N_1 \\ N_2 \end{bmatrix} = \begin{bmatrix} A_{11} & A_{12} \\ A_{12} & A_{22} \end{bmatrix} \begin{bmatrix} \varepsilon_1^0 \\ \varepsilon_2^0 \end{bmatrix} - \begin{bmatrix} N_1^T \\ N_2^T \end{bmatrix} \tag{45}$$

where

$$N_i = \int_{-h/2}^{h/2} \sigma_i \, dx, \quad N_i^T = \int_{-h/2}^{h/2} Q_{ik}\alpha_k \Delta T \, dx$$

$$\left\langle \begin{matrix} i, j = 1, 2 \\ k = 1, 2, 6 \end{matrix} \right\rangle$$

$$A_{ij} = \int_{-h/2}^{h/2} Q_{ij} \, dx$$

In addition, $\alpha_k$ are the ply thermal expansion coefficients. Ply stresses are calculated from the local constitutive relations

$$\sigma_i = Q_{ij}(\varepsilon_j^0 - \alpha_j) \qquad \langle i, j = 1, 2, 6 \rangle \tag{46}$$

The data reduction was accomplished in two stages and the results superimposed. First, the residual stresses were calculated using the following initial ply properties

$$\begin{gathered} E_L = 20 \text{ Msi}, E_T = 1.3 \text{ Msi}, G_{LT} = 0.8 \text{ Msi} \\ \nu_{LT} = 0.3, \alpha_T = -0.5 \times 10^6/°F, \alpha_T = 14 \times 10^6/°F, \Delta T = -280°F \end{gathered} \tag{47}$$

where as in eq. (44) the subscripts L and T refer to a coordinate system parallel and transverse to the fibers. Thermal expansion coefficients in the longitudinal and transverse directions are denoted by $\alpha_L$ and $\alpha_T$, respectively. The value of $\Delta T$ is chosen as the difference between room temperature and cure temperature. For mechanical stresses the 0° secant modulus, $E_1$, at failure is utilized, while the other elastic properties are assumed to be constant. Since the core is not co-cured with the face sheets, thermal stresses are based on cure of the face sheets independent of the core.

For mechanical stresses the longitudinal compression secant modulus of the unidirectional ply and the compression secant modulus of the core at failure are used due to the nonlinear response of these properties. Other elastic properties are assumed to be constant. The Poisson's ratio of the core is assumed to be $\nu = 0.35$. In the determination of mechanical stresses, $N_i^T$ and $N_2$ (i.e. the load is applied in the $x_1$ direction) are allowed to vanish. Typical stress-strain curves in compression for the core and a unidirectional composite are shown in Figs 8 and 9, respectively. Because most of the load is carried by the unidirectional face sheets, the nonlinear response seen in Fig. 9 is due primarily to the

compression response of the 0° composite.

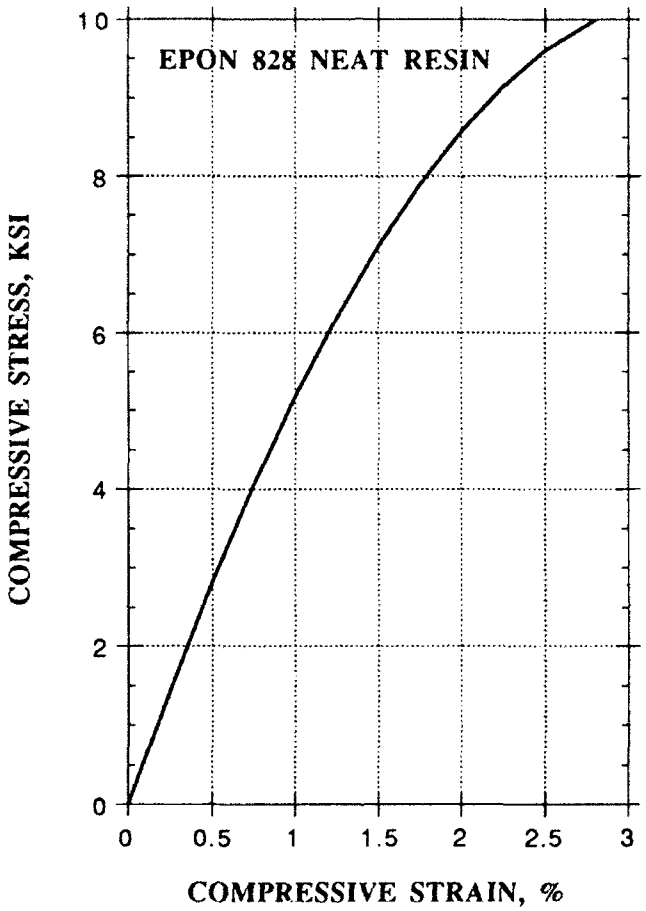


**Fig. 8 Compressive Stress-Strain Curve for Neat Epon 828 Resin**

## Results and Discussion

Experimental results are shown in Table 3. All data are extrapolated to 60% fiber volume. The compression strength of the face sheet in the x and y directions are denoted

by $S_{xf}$, and $S_{yf}$, respectively, while the 0° ply stresses at failure (including thermal residual

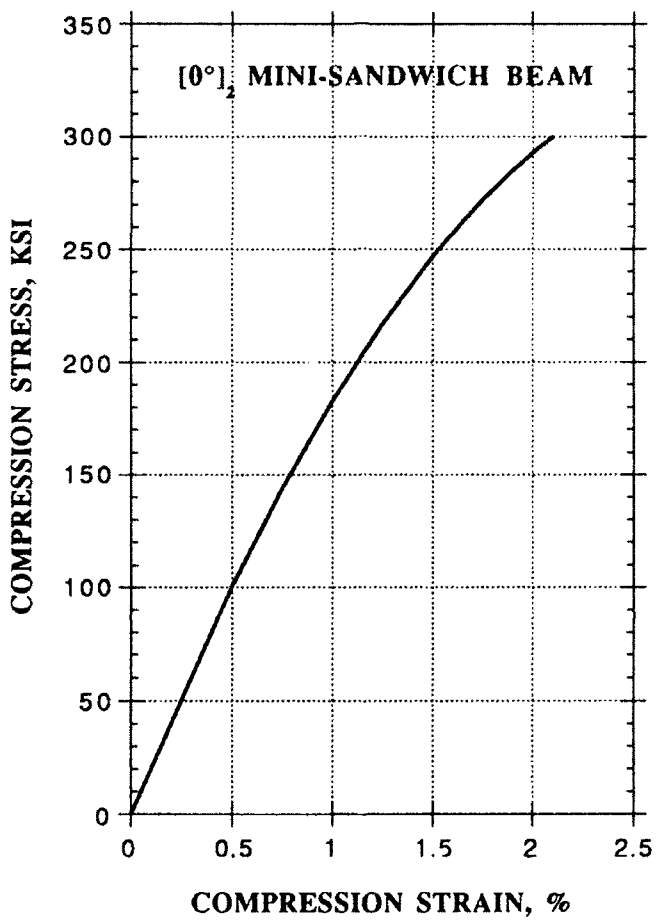


**Fig. 9 Stress-Strain Curve for 0° Mini-Sandwich Beam**

stresses) in the longitudinal and transverse directions are denoted by $\sigma_L$ and $\sigma_T$, respectively. Longitudinal and transverse residual stresses of the 0° plies are denoted by $\sigma_L{}^T$ and $\sigma_T{}^T$, respectively. Note that due to a mismatch between the effective Poisson's ratio, $\nu_{xy}$, of the face sheet and the core, the face sheets will be under biaxial inplane normal stresses at the macroscopic (laminate) level. In addition, there are no inplane shear

stresses present in the 0° plies. Thus, the unidirectional plies are only subjected to biaxial normal stresses inplane. Results for the $[0/45/90/-45]_S$ face sheets are not shown, as the initial failure was due to free-edge delamination which reduced the apparent compression strength considerably.

**TABLE 3 Experimental Data, psi**

| Laminate | $S_{xf}$ | $S_{yf}$ | $\sigma_L$ | $\sigma_T$ | $\sigma_L{}^T$ | $\sigma_T{}^T$ |
|---|---|---|---|---|---|---|
| $[90°]_{24}$* | -32,800 | 0 | 0 | -32,800 | 0 | 0 |
| $[0°]_2$ | -281,550 | 765 | -281,550 | 765 | 0 | 0 |
| $[0°/90°]_S$ | -141,750 | 7,964 | -262,680 | -213 | -4,780 | 4,780 |
| $[\pm45°/0°/90°]_S$ | -103,745 | 454 | -260,680 | 5,027 | -4,780 | -4,780 |
| $[0°_2/\pm30°]_S$ | -135,145 | -3,241 | -166,340 | 8,255 | 4,564 | 1,966 |
| $[0°/\pm60°]_S$ | -97,208 | 740 | -290,612 | 5,215 | -4,780 | 4,780 |

*Solid laminate tested for transverse compression strength

Experimental results from Table 3 were compared to the Tsai-Wu failure criterion, eq. (44). For the ply loading under consideration, eq. (44) reduces to the form

$$\frac{\sigma_L{}^2}{S_{LT}\,S_{LC}} + \frac{\sigma_T{}^2}{S_{TT}\,S_{TC}} - \frac{\sigma_L\,\sigma_T}{2\sqrt{S_{LT}\,S_{LC}\,S_{TT}\,S_{TC}}} + \left(\frac{1}{S_{LT}} - \frac{1}{S_{LC}}\right)\sigma_L + \left(\frac{1}{S_{TT}} - \frac{1}{S_{TC}}\right)\sigma_T = 1 \tag{48}$$

The following ply strength parameters were used in comparing theory and experiment:

$$S_{LT} = 250 \text{ ksi},\ S_{LC} = 282 \text{ ksi},\ S_{TT} = 7.5 \text{ ksi},\ S_{TC} = 33 \text{ ksi} \tag{49}$$

A comparison between eq. (48) and the experimental data is shown in Fig. 10. Except for the results of the $[0°_2/\pm30°]_S$ laminate, the longitudinal compression strength appears to be relatively insensitive to transverse load. In the case of the $[0°_2/\pm30°]_S$ laminate the

transverse tensile stress, $\sigma_T$, exceeds the transverse tensile strength, $S_{TT}$. When transverse tensile failure occurs first, the fibers lose support from the matrix and fiber buckling becomes the failure mode. For the other laminates the predominant failure mode appears to be shear failure of the fiber as previously described by Crasto and Kim [2]. Thus if $\sigma_T < S_{TT}$, then little or no interaction exists between longitudinal compression strength and transverse tensile loading. One caution must be raised here, however, because the laminate geometries presented here do not induce transverse compression in the 0° plies (when thermal residual stresses are included), other than the very small transverse compression stress present in the $[0°/90°]_S$ laminate.

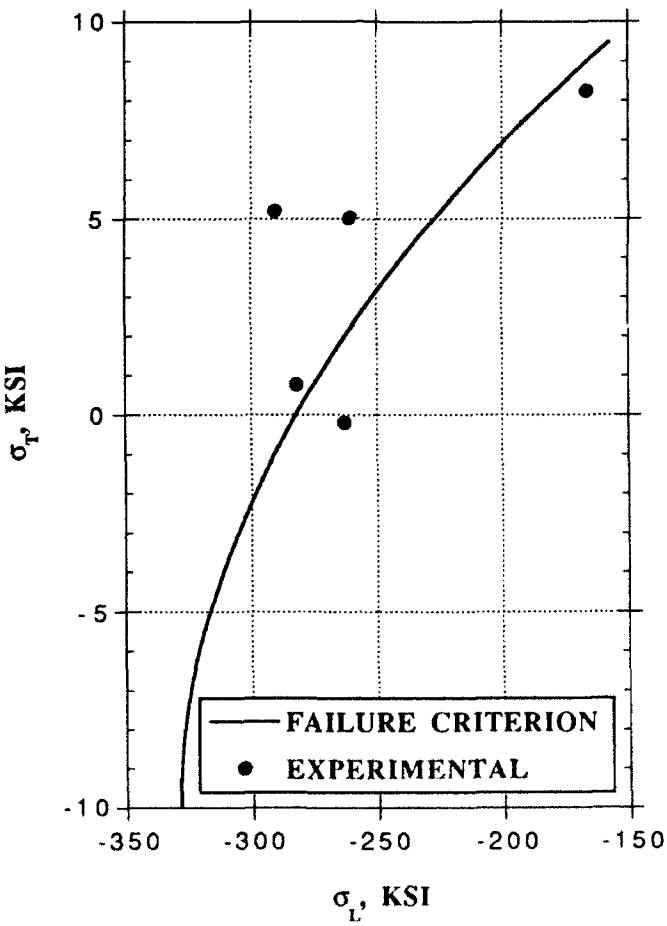


**Fig. 10 Comparison Between Eq. (48) and Data in Table 3**

Thus a meaningful conclusion cannot be made concerning the interaction between longitudinal compression and transverse compression. Such data is very difficult to obtain in flat laminates, leaving combined axial compression and external pressure loading of tubular specimens as the only likely means of generating this information.

It is also important to note that 0° compression strength is very high and carries over to laminate in-situ unidirectional plies.

## 3. STRESS ANALYSIS MODELS FOR THICK COMPOSITES

It is well recognized that shear deformation can be more significant in laminated, anisotropic plates than in isotropic, homogeneous plates. This is due to the large ratios of effective inplane tensile moduli to through-the-thickness shear moduli. Shear deformation theories based on Mindlin's assumptions [4] have been developed for laminated, anisotropic plates [5, 6]. A theory has also been developed [7] for the bending of laminated, anisotropic plates which includes the effects of transverse shear deformation in a manner similar to Reissner's theory for homogeneous, isotropic plates [8]. This theory is based on Reissner's principle [9] in a modified form which requires assumed distributions of interlaminar shear stresses in addition to the inplane displacements. This theory has been modified [10] to include the effect of transverse normal stress without increasing the number of bending equations above those generated in classical shear deformation theory. In this theory the interlaminar normal stress distribution is assumed, in addition to the interlaminar shear stress distributions. Numerical results for cylindrical bending of laminated, anisotropic plates subjected to a half sine wave lateral load showed that improved results for bending deflections can be obtained by including transverse normal stress effects as well as transverse shear deformation effects. These numerical results were obtained for simply-supported boundary conditions and results compared to exact solutions from classical theory of elasticity.

In the present effort the effect of transverse shear and normal stresses on the bending of symmetrically laminated, anisotropic plates subjected to cylindrical bending under uniform lateral load is investigated. Closed form solutions are developed for simply-supported boundary conditions.

### Modified Shear Deformation Theory

For continuity purposes, some of the details in the development of the field equations developed by Whitney and Rose [10] will be outlined here. Consider a rectangular laminated plate of thickness h with a symmetric stacking sequence relative to the plate midplane. Each ply is constructed of an orthotropic material with the principle axis of orthotropy oriented at an arbitrary angle, $\theta$, relative to the x-axis of the plate. The inplane displacements are assumed to be of the form

$$u = u^0(x, y) + z\,\psi_x(x, y), \quad v = v^0(x, y) + z\,\psi_y(x, y) \tag{50}$$

while the plate deflection, w, is expressed in terms of the weighted displacement

$$w^* = \frac{3}{2h} \int_{-h/2}^{h/2} w(x, y, z) \left[1 - 4 \left(\frac{z}{h}\right)^2\right] dz \tag{51}$$

The ply constitutive equations are of the form

$$\sigma_i = C_{ik}\varepsilon_k, \quad \varepsilon_j = S_{jk}\sigma_k \tag{52}$$

where $C_{ik}$ and $S_{jk}$ are the stiffnesses and compliances, respectively. We now eliminate the interlaminar normal strain $\varepsilon_3$ by utilizing the first of the constitutive relations, eq. (52), in the form

$$\sigma_i = Q_{ik}\varepsilon_k + \frac{C_{i3}}{C_{33}}\sigma_3 \qquad (i, k = 1, 2, 6) \tag{53}$$

where $Q_{ij}$ are, as previously, the reduced stiffnesses for plane stress given by the relationship

$$Q_{ik} = C_{ik} - \frac{C_{i3}C_{k3}}{C_{33}}$$

Reissner's principle is written in terms of the variational equation $\delta\Pi = 0$. Omitting boundary and surface traction terms for simplicity, the variational function $\delta\Pi$ can be written in the modified form [10]

$$\begin{aligned} \delta\Pi = \int_V \{ & [\sigma_i - (Q_{ij}\varepsilon_j + \frac{C_{i3}}{C_{33}}\sigma_3)]\, \delta\varepsilon_i + (\varepsilon_j - S_{km}\sigma_m)\, \delta\sigma_j \\ & + (\sigma_{1,1} + \sigma_{6,2} + \sigma_{5,5})\, \delta u + (\sigma_{6,1} + \sigma_{2,2} + \sigma_{4,4})\, \delta v \qquad \left\langle \begin{matrix} i, j = 1, 2, 6 \\ k, m = 4, 5 \end{matrix} \right\rangle \\ & (\sigma_{5,1} + \sigma_{4,2} + \sigma_{3,3})\, \delta w \,\}\, dV \end{aligned} \tag{54}$$

where a repeated index denotes summation and, in the usual manner, $\sigma_i$ and $\varepsilon_i$ denote the stress and strain components, respectively. Using conventional nomenclature, the subscripts 1, 2, and 3 here denote, x, y, and z, respectively while 4, 5, and 6 correspond to yz, xz, and xy, respectively.

We now denote normal stresses, shear stresses, normal strains, and shear strains by $\sigma_i$, $\tau_{ij}$, $\varepsilon_i$ and $\gamma_{ij}$, respectively. In order to implement eq. (54), we need to assume a distribution through the thickness for $\tau_{xz}$, $\tau_{yz}$, and $\sigma_z$. As in the original work by Whitney and Rose [10], we assume these stress components to be of the same form as utilized by Reissner [8] for homogeneous, isotropic plates, namely

$$\begin{aligned} \tau_{xz} &= [1 - 4 (\tfrac{z}{h})^2] \frac{3Q_x}{2h} \\ \tau_{yz} &= [1 - 4 (\tfrac{z}{h})^2] \frac{3Q_y}{2h} \\ \sigma_z &= \frac{1}{2} \{ [3 - 4 (\tfrac{z}{h})^2] (\tfrac{z}{h}) (p_1 - p_2) + (p_1 + p_2) \} \end{aligned} \tag{55}$$

where $Q_x$ and $Q_y$ are the shear force resultants defined in the usual manner

$$(Q_x, Q_y) = \int_{-h/2}^{h/2} (\tau_{xz}, \tau_{yz})\, dz$$

and

$$p_1 = \sigma_z(h/2), \quad p_2 = \sigma_z(-h/2)$$

These relationships are consistent with linear inplane stresses through-the-thickness for the case of homogeneous plates. It should be noted that the incorporation of $\sigma_z$ in the constitutive relations, eq. (53), will induce some nonlinearity through-the-thickness with regard to the inplane stresses. This may be of little consequence, however, in obtaining macroscopic response of the laminate. Detailed local interlaminar stress distributions require integration of the equations of equilibrium in conjunction with the inplane stresses as determined from the laminated plate theory.

Substituting eqs. (50), (51), and (55) into eq. (54), we obtain the following inplane constitutive relations in terms of force resultants and moments

$$\begin{aligned} N_i &= A_{ij}\, \varepsilon_j + L_i\, (p_1 + p_2) \\ M_i &= D_{ij}\, \kappa_j + J_i\, (p_1 - p_2) \end{aligned} \qquad (i, j = 1, 2, 6) \tag{56}$$

where

$$(N_i, M_i) = \int_{-h/2}^{h/2} \sigma_i (1, z)\, dz, \quad (A_{ij}, D_{ij}) = \int_{-h/2}^{h/2} Q_{ij} (1, z^2)\, dz$$

$$L_i = \frac{1}{2}\int_{-h/2}^{h/2} \frac{C_{i3}}{C_{33}}\, dz, \quad J_i = \frac{1}{2}\int_{-h/2}^{h/2} \frac{C_{i3}}{C_{33}} (\frac{z}{h})[3 - 4 (\frac{z}{h})^2]\, z\, dz$$

We note in eq. (56) that the inplane force resultants are coupled to the lateral surface tractions. Thus, the midplane strains do not vanish in the case of the bending due to lateral load when the effects of transverse normal stress are considered. Reissner [8] did not consider midplane strains in the development of his theory for homogeneous, isotropic plates. In a similar manner we obtain the constitutive relations for the transverse shear force resultants, $Q_x$ and $Q_y$, from eq. (54) with the result

$$\begin{bmatrix} Q_x \\ Q_y \end{bmatrix} = \begin{bmatrix} F_{55} & F_{45} \\ F_{45} & F_{44} \end{bmatrix} \begin{bmatrix} \psi_x + w^*_{,x} \\ \psi_y + w^*_{,y} \end{bmatrix} \tag{57}$$

where

$$F_{44} = \frac{R_{55}}{(R_{44} R_{55} - R_{45}^2)}, \quad F_{55} = \frac{R_{44}}{(R_{44} R_{55} - R_{45}^2)}, \quad F_{45} = -\frac{R_{45}}{(R_{44} R_{55} - R_{45}^2)}$$

and

$$R_{ij} = \frac{9}{4h^2}\int_{-h/2}^{h/2} S_{ij} [1 - 4 (\frac{z}{h})^2]^2\, dz \qquad (i, j = 4, 5)$$

Here $S_{ij}$ denotes the anisotropic transverse shear compliances.

The equilibrium equations in terms of force and moment resultants can be obtained from the last three terms in eq. (5) with the result

$$\begin{aligned} N_{x,x} + N_{xy,y} &= 0 \\ N_{xy,x} + N_{y,y} &= 0 \\ M_{x,x} + M_{xy,y} - Q_x &= 0 \\ M_{xy,x} + M_{y,y} - Q_y &= 0 \\ Q_{x,x} + Q_{y,y} + (p_1 - p_2) &= 0 \end{aligned} \tag{58}$$

These five equations could be expressed in terms of the displacement variables $u^0$, $v^0$,

$\psi_x$, $\psi_y$, and $w^*$ by utilizing the constitutive relations, eqs. (56) and (57). The boundary conditions are those of classical shear deformation theory as applied to laminated plates [6].

## Cylindrical Bending Under Uniform Lateral Load

For cylindrical bending we consider a symmetric laminate where the length in the y-direction is much longer than the x-direction, as illustrated in Fig. 11. If the laminate is subjected to a lateral load which is independent of y, then the resulting deformations will be independent of y. Such cases are referred to as cylindrical bending.

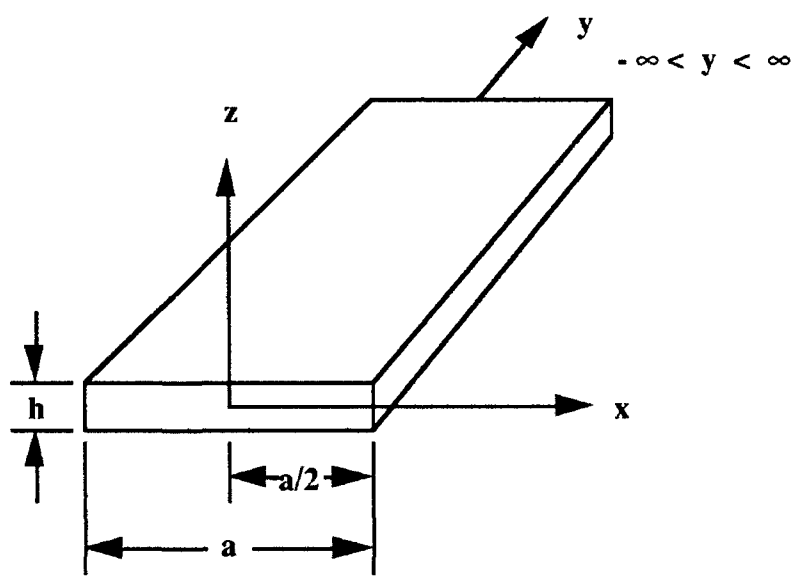


**Fig. 11 Cylindrical Bending**

The displacements in eq. (1) and (2) now take the form

$$u^0 = U(x),\ v^0 = V(x),\ \psi_x = \Psi_x(x),\ \psi_y = \Psi_y(x),\ w^* = W(x) \tag{59}$$

Denoting differentiation with respect to x by a prime, the first two equilibrium equations in (58) reduce to the following

$$N_x' = 0, \quad N_{xy}' = 0 \tag{60}$$

which leads to constant values of $N_x$ and $N_{xy}$. Combining eq. (60) with the constitutive relations, eqs. (56) and (57), and substituting the results into the last three equations in (58), we obtain the following bending equations

$$\begin{aligned} D_{11}\,\Psi_x'' - F_{55}\,\Psi_x + D_{16}\,\Psi_y'' - F_{45}\,\Psi_y - F_{55}\,W' + J_1\,(p_1' - p_2') &= 0 \\ D_{16}\,\Psi_x'' - F_{45}\,\Psi_x + D_{66}\,\Psi_y'' - F_{44}\,\Psi_y - F_{45}\,W' + J_6\,(p_1' - p_2') &= 0 \\ F_{55}\,\Psi_x' + F_{45}\,\Psi_y' + F_{55}\,W'' + (p_1 - p_2) &= 0 \end{aligned} \tag{61}$$

For a uniform load

$$p_1 = p_0 = \text{constant}, \quad p_2 = 0 \tag{62}$$

Because the lateral load is constant, the effect of transverse normal stress vanishes from the first two equations in (61), with the result

$$\begin{aligned} D_{11}\,\Psi_x'' - F_{55}\,\Psi_x + D_{16}\,\Psi_y'' - F_{45}\,\Psi_y - F_{55}\,W' &= 0 \\ D_{16}\,\Psi_x'' - F_{45}\,\Psi_x + D_{66}\,\Psi_y'' - F_{44}\,\Psi_y - F_{45}\,W' &= 0 \\ F_{55}\,\Psi_x' + F_{45}\,\Psi_y' + F_{55}\,W'' + p_0 &= 0 \end{aligned} \tag{63}$$

The solution to eqs. (63) is given by

$$\psi_x = c_1 + c_2 x + \frac{c_3}{2}x^2 - \frac{D_{16}}{D_{11}}\left(A\cosh\lambda\frac{x}{h} + B\sinh\lambda\frac{x}{h}\right) - \frac{p_0}{6D_{11}}x^3$$

$$\psi_y = H_1\left(c_3 - \frac{p_0}{D_{11}}\right) + A\cosh\lambda\frac{x}{h} + B\sinh\lambda\frac{x}{h} \tag{64}$$

$$\begin{aligned} w = c_4 - c_1 x - \frac{c_2}{2}x^2 + (6H_3 - x^2)\frac{c_3}{6}x - (12H_2 - x^2)\frac{p_0}{24D_{11}}x^2 \\ + \frac{hH_3}{\lambda}\left(A\sinh\lambda\frac{x}{h} + B\cosh\lambda\frac{x}{h}\right) \end{aligned}$$

where

$$\lambda = \sqrt{\frac{(F_{44}F_{55} - F_{45}^2)D_{11}h^2}{F_{55}(D_{11}D_{66} - D_{16}^2)}}, \quad H_1 = \frac{(F_{55}D_{16} - F_{45}D_{11})}{(F_{44}F_{55} - F_{45}^2)}$$

$$H_2 = \frac{(F_{44}D_{11} - F_{45}D_{16})}{(F_{44}F_{55} - F_{45}^2)}, \quad H_3 = \frac{(F_{55}D_{16} - F_{45}D_{11})}{F_{55}D_{11}}$$

The width of the plate is denoted by a and the axis system is placed at the middle such that the boundaries are located at $x = \pm a/2$ (see Fig. 11). At the laminate level, transverse normal stress will only effect cases in which force and/or moment boundary conditions are required. In particular, because transverse normal stress effects do not appear in eqs. (63), they enter the problem through force and/or moment boundary conditions, as observed in the constitutive relations, eqs. (56). Thus, for example, in the case of clamped boundaries, which involves displacement conditions only, transverse normal stress effects will not be present at the laminate level. Transverse normal stress will, however, have an effect on the ply stresses by virtue of eq. (53).

We now consider simply-supported boundary conditions. For this case w will be symmetric about $x = 0$, while both $\psi_x$ and $\psi_y$ are anti-symmetric. This leads to the result

$$c_1 = c_3 = A = 0 \tag{65}$$

For simply-supported boundaries, we require that at $x = \pm a/2$

$$w = M_x = M_{xy} = N_x = N_{xy} = 0 \tag{66}$$

where, from the constitutive relations, eqs. (66)

$$\begin{aligned} M_x &= D_{11}\psi_{x,x} + D_{16}\psi_{y,x} + J_1 p_0 \\ M_{xy} &= D_{16}\psi_{x,x} + D_{66}\psi_{y,x} + J_6 p_0 \end{aligned} \tag{67}$$

Combining eqs. (64) and (67), we find that

$$c_2 = \frac{(8H_1D_{16} + D_{11}a^2 - 8J_1D_{11})}{8D_{11}^2} p_0, \quad B = \frac{h}{D_{11}\lambda \cosh \lambda\frac{a}{2h}} [H_1 - \frac{D_{11}(J_6D_{11} - J_1D_{16}}{(D_{11}D_{66} - D_{16}^2)}] p_0$$

$$c_4 = \{[48(H_2D_{11} + H_1D_{16} - J_1D_{11}) + D_{11}a^2]\lambda a - 384h^2H_3D_{11}[H_1 - \frac{D_{11}(J_6D_{11} - J_1D_{16}}{(D_{11}D_{66} - D_{16}^2)}]\} \frac{p_0}{384\lambda^2 D_{11}^2} \tag{68}$$

The maximum deflection will occur at the center of the plate, x = 0, and can be written in the form

$$w_{max} = w_{CLPT}(1 + \frac{H}{5}) \tag{69}$$

where

$$H = \frac{48}{a^2}(H_2 + \frac{D_{16}}{D_{11}}H_1 - J_1) - \frac{384h^2H_3}{\lambda^2a^4}[H_1 - \frac{D_{11}(J_6D_{11} - J_1D_{16})}{(D_{11}D_{66} - D_{16}^2)}](\frac{\cosh \lambda\frac{a}{2h} - 1}{\cosh \lambda\frac{a}{2h}})$$

and $w_{CLPT}$ is the maximum deflection as determined from classical laminated plate theory with shear deformation and transverse normal stress effects neglected and is of the form

$$w_{CLPT} = \frac{5a^4}{384D_{11}} p_0 \tag{70}$$

Thus, the term H contains the effects of both transverse shear deformation and transverse normal stress. We note that the classical solution is independent of the bending-twisting coupling stiffness $D_{16}$. For the case of an orthotropic material $F_{45} = D_{16} = 0$ and eq. (69) reduces to

$$w_{max} = w_{CLPT}[1 + \frac{48(D_{11} - J_1F_{55})}{5F_{55}a^2}] \tag{71}$$

We should also note that midplane strains will also occur. Combining the boundary conditions, eq. (66), with eq. (60), we find that

$$N_x = N_{xy} = 0 \tag{72}$$

throughout the plate. Substituting eq. (72) into the first of the constitutive relations, eq. (56), we obtain the midplane strains

$$\varepsilon_x{}^0 = \frac{(A_{66}L_1 - A_{16}L_6)}{(A_{11}A_{66} - A_{16}{}^2)}$$
$$\gamma_{xy}{}^0 = \frac{(A_{11}L_6 - A_{16}L_1)}{(A_{11}A_{66} - A_{16}{}^2)} \tag{73}$$

## Numerical Results

We now consider laminates with the stacking geometry $[0°/90°]_S$ and $[\pm 45°]_S$ having the following unidirectional properties

$$E_L/E_T = 14,\ G_{LT}/E_T = G_{L3}/E_T = 0.615,\ G_{T3}/E_T = 0.323,$$
$$\nu_{LT} = \nu_{L3} = 0.3,\ \nu_{T3} = 0.55 \tag{74}$$

where the subscript L, T, and 3 denote axes parallel to the fiber, perpendicular to the fiber, and through-the-thickness of a unidirectional composite, respectively. In addition $E_i$, $G_{ij}$, and $\nu_{ij}$ denote the Young's modulus in the ith direction, the shear modulus relative to the i-j

**TABLE 4 Maximum Deflection**
**$w_{max}/w_{CLPT}$**

| | $[0°/90°]_S$ | | $[\pm 45°]_S$ | |
|---|---|---|---|---|
| **a/h** | $w_{SN}$ | $w_{SD}$ | $w_{SN}$ | $w_{SD}$ |
| 5 | 1.901 | 1.923 | 1.421 | 1.442 |
| 10 | 1.225 | 1.231 | 1.107 | 1.112 |
| 20 | 1.056 | 1.058 | 1.027 | 1.028 |
| 30 | 1.025 | 1.026 | 1.012 | 1.013 |

plane, and the Poisson's ratio measured by contraction in the jth direction during a uniaxial tensile test in the ith direction, respectively. These properties represent state-of-the-art unidirectional graphite/epoxy composites.

Numerical results are shown in Table 4 for the maximum deflection. Equation (71) is applicable to the $[0°/90°]_S$ stacking geometry, while eq. (20) is required for the anisotropic $[\pm 45°]_S$ laminate. The normalized deflection, $w_{SN}$, represents eqs. (69) and (71) with both shear deformation and normal stress effects included, while $w_{SD}$ represents these same equations with normal stress effects neglected ($J_1 = J_6 = 0$).

## Discussion

A cursory examination of table 1 reveals that the inclusion of transverse normal stress reduces the maximum deflection compared to shear deformation. This is consistent with the results presented by Whitney and Rose [10] where comparison with exact elasticity solutions showed that shear deformation alone overestimated the maximum deflection. The inclusion of both shear deformation and transverse normal stress, in the same manner presented here, gave almost identical results to exact elasticity.

The effect of shear deformation and transverse normal stress is more severe in the $[0°/90°]_S$ laminate than in the $[\pm 45°]_S$ stacking geometry. This is anticipated as the $[0°/90°]_S$ laminate has a higher effective inplane modulus to interlaminar shear modulus ratio than the $[\pm 45°]_S$ angle-ply composite.

## REFERENCES


1. Tsai, S. W. and Hahn, H. T. *Introduction to Composite Materials*, Technomic Publishing Co., Lancaster, PA, 1980.

2. Theocaris, P. S., "Positive and Negative Failure-Shears in Orthotropic Materials," *Journal of Reinforced Plastics and Composites*, Vol. 11, No. 1, 1992, pp. 32-55.

3. Crasto, A. and Kim, R. Y., "Compression Strengths of Advanced Composites from a Mini-Sandwich Beam," *Proceedings of the 22nd International SAMPE Technical Conference*, Society for Advanced Manufacturing and Processing Engineers, Covina, CA, 1990, pp. 264-277.

4. Mindlin, R. D., "Influence of Rotatory Inertia and Shear on Flexural Motions of Isotropic, Elastic Plates," *Journal of Applied Mechanics*, Vol. 18, 1951, pp. 336-343.

5. Yang, P. C., Norris, C. H., and Stavsky, Y., "Elastic Wave Propagation in Heterogeneous Plates," *International Journal of Solids and Structures*, Vol. 2, 1966, pp. 665-684.

6. Whitney, J. M., and Pagano, N. J. "Shear Deformation in Heterogeneous Anisotropic Plates", *Journal of Applied Mechanics*, Vol. 37, 1970, pp. 1031-1036.

7. Whitney, J. M., "A Modified Shear Deformation Theory for Laminated Anisotropic Plates", *Proceedings of the American Society for Composites, Fifth Technical Conference*, Technomic Publishing Co., Lancaster, PA, 1990, pp. 469-478.

8. Reissner, E., "The Effect of Transverse Shear Deformation on the Bending of Elastic Plates," *Journal of Applied Mechanics*, Vol. 12, 1945, pp. 69-77.

9. Reissner, E., "On a Variational Theorem in Elasticity," *Journal of Mathematics and Physics*, Vol. 29, 1950, pp. 90-97.

10. Whitney, J. M., and Rose, D. H., "Effect of Transverse Normal Stress on the Bending of Thick Laminated Plates," *Proceedings of ICCM VIII*, Edited by S. W. Tsai and G. S. Springer, Society for the Advancement of Material and Process Engineering

(SAMPE), Covina, CA, 1991, pp. 30-B-1 - 30-B-10.